Progress In Electromagnetics Research M, Vol. 114, 79–89, 2022

Scattering from a 90° Metallic Wedge with One Face Coated by a Double Negative Metamaterial Layer

Giovanni Riccio[1, *], Gianluca Gennarelli[2], Flaminio Ferrara[3], Claudio Gennarelli[3], and Rocco Guerriero[3]

Abstract—This manuscript refers to the electromagnetic scattering problem involving plane waves at skew incidence with respect to the edge of a right-angled metallic wedge having one face coated by a double negative metamaterial sheet. Its presence in the propagation scenario is properly accounted at high frequencies by considering the geometrical optics response of the structure and the diffraction contribution arising from the edge of the wedge. In particular, the reflection coefficients related to the coated surface are determined for both the polarizations by using the equivalent transmission line circuit, whereas the diffraction coefficients are obtained by applying the uniform asymptotic physical optics approach. This last is based on electric and magnetic equivalent surface currents under the physical optics approximation and permits to evaluate the diffraction contribution in the context of the uniform geometrical theory of diffraction. The resulting approximate solution is characterized by the same simplicity of use of the heuristic solutions and provides reliable field values as confirmed by the numerical tests carried out by a full-wave commercial software.

1. INTRODUCTION

This research work presents a useful high-frequency solution for studying the plane wave scattering from a metallic wedge that is partially coated by a double negative metamaterial (DNG MTM) layer. The material coating of metallic structures is a procedure widely used in many application contexts of interest to the antennas and propagation community. In fact, this surface treatment allows one to modify the interactions with electromagnetic waves (f.i., aircrafts and naval ships can require proper material covering over their otherwise metallic surfaces to control their radar cross section) as well as to design more efficient antenna systems and to manipulate the propagation in microwave and optical devices.

A DNG MTM is characterized by negative real parts of permittivity and permeability as well as by negative refraction index at the frequencies of interest, and consequently, it is also known as negative index materials (NIMs) or left-handed materials (LHMs) or backward (BW) media (see [1–4] for information about characteristics and applications as well as additional references). Previous terms account for the unconventional characteristics of such artificial materials, f.i., LHM is related to the mutual position of electric field, magnetic field, and wave vector of a propagating plane wave, and BW is associated with the backward propagation with the wave vector antiparallel to the Poynting one.

Accounting for the increasing interest, research activities as well as industrial, space and military applications can take advantage of techniques for the evaluation of the electromagnetic scattering from

Received 27 September 2022, Accepted 31 October 2022, Scheduled 15 November 2022

* Corresponding author: Giovanni Riccio (griccio@unisa.it).

[1] Department of Information and Electrical Engineering and Applied Mathematics, University of Salerno, via Giovanni Paolo II, 132, 84084 Fisciano (SA), Italy. [2] Institute for Electromagnetic Sensing of the Environment, National Research Council, via Diocleziano 328, 80124 Naples, Italy. [3] Department of Industrial Engineering, University of Salerno, via Giovanni Paolo II, 132, 84084 Fisciano (SA), Italy.

composite structure hosting DNG MTMs. Analytical asymptotic methods and numerical techniques can be used, but the latter necessitates more and more computational resources to obtain reliable results when the frequency grows. Some asymptotic analytical approaches, such as the Uniform Geometrical Theory of Diffraction (UTD) [5], work efficiently at high frequencies and provide a physically appealing ray propagation theory including the diffraction contribution in addition to the Geometrical Optics (GO) ones for the scattering evaluation. Many research activities in the UTD framework have furnished solutions for two- and three-dimensional scattering problems involving coated perfect electrically conducting (PEC) objects (see [6–10] for a limited and non-exhaustive list of references). Note that the presence of thin material coatings has been taken into account by adopting an impedance boundary condition (see also [11]). Further analytical methods based on the reduction of the scattering problem to integral equations have been proposed in [12, 13]. Moreover, the UTD solution for a PEC wedge [5] has been heuristically generalized in [14–16] to account for the impedance boundary conditions. An analytical solution for the diffraction of plane waves by a right angle impedance wedge which is lying between double negative and positive materials has been investigated in [17].

An alternative asymptotic analytical solution in the UTD context has been presented in [18] to handle the diffraction by a planar junction consisting of double positive (DPS) and DNG MTM layers with PEC backing when a plane wave hits the composite structure at skew incidence with respect to the discontinuity. Such an approximate solution has been obtained by applying the Uniform Asymptotic Physical Optics (UAPO) approach based on the PO approximation of electric and magnetic equivalent surface currents radiating in the upper half-space surrounding the structure. Note that the elements of the resulting matrix formulation are expressed in closed form and involve local reference systems, UTD transition function [5], and the GO response of the structure in terms of reflection coefficients. The last have been determined for both the polarizations by using the equivalent transmission line (ETL) models. Accordingly, the UAPO solution is easy to handle and reduces computation and time resources with respect to numerical techniques and analytical methods involving the calculation of differential/integral equations or special functions. The corresponding diffracted field compensates the jumps of the GO field at the shadow boundaries and contributes to reliable results as confirmed by the numerical tests. Obviously there are also some cons. The well-known limitations of the PO-based techniques and the absence of the surface waves in the UAPO approach can decrease the accuracy of the estimated field values in particular cases, e.g., incidence directions close to the grazing one [18]. Other canonical problems solved by means of the UAPO approach can be found in [19–30].

This manuscript is organized as follows. Section 2 contains the expressions of the PO surface currents located on the external faces and used as radiating sources in the subsequent section, where the UAPO approach is exploited to obtain a solution for evaluating the plane wave diffraction in the case of skew incidence (see Fig. 1). Section 4 includes comparisons with Comsol Multiphysics® data to assess the effectiveness of the proposed solution. Conclusions are reported in Section 5.

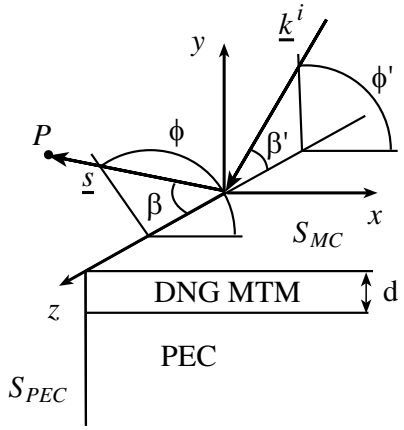

Figure 1. A particular DNG MTM-coated PEC wedge is lit by an incident plane wave.

2. THE PO RADIATING SOURCES

A lossy planar DNG MTM layer with thickness d covers the top surface of a 90° metallic wedge as depicted in Fig. 1. The hosting wedge is assumed to be a PEC object at the frequency of interest, and the DNG MTM coating is characterized by permittivity $\varepsilon = -\varepsilon_0(\varepsilon' + j\varepsilon'') = \varepsilon_0\varepsilon_r$ and permeability $\mu = -\mu_0(\mu' + j\mu'') = \mu_0\mu_r$, where ε', ε'', μ', μ'' are positive quantities, and ε_0, μ_0 are related to the free space. The external surface S_{MC} of the DNG MTM layer contains the xz-plane of the reference system having the z-axis coincident with the edge, whereas the uncovered PEC surface is denoted by S_{PEC}.

An incident plane wave with the electric field $\underline{E}_0^i \exp(-j\underline{k}^i \cdot \underline{r})$ propagates according to $\underline{k}^i = k_0\hat{k}^i = k_0(-\sin\beta'\cos\phi'\hat{x} - \sin\beta'\sin\phi'\hat{y} + \cos\beta'\hat{z})$, where k_0 is the free-space propagation constant, and the incidence direction is defined by the angles β' and ϕ'. The vector $\underline{r}$ symbolizes the position of the observation point P, and $\underline{E}_0^i$ can be expressed in terms of its components with respect to the ordinary plane of incidence, i.e., $\underline{E}_0^i = E_{TM}^i\hat{u}_{TM} + E_{TE}^i\hat{u}_{TE}$ with $\hat{u}_{TM} = \hat{u}_{TE} \times \hat{k}^i$ and $\hat{u}_{TE} = (\hat{k}^i \times \hat{n})\Big/|\hat{k}^i \times \hat{n}|$, $\hat{n}$ being the unit vector normal to the surface.

The electric PO surface current $\underline{J}_{s_{PEC}}$ on S_{PEC} can be so expressed:

$$\begin{aligned}\underline{J}_{s_{PEC}} &= \frac{2}{\zeta_0}\left[E_{TM_{PEC}}^i\hat{t}_{PEC} - E_{TE_{PEC}}^i\sin\beta'\cos\phi'\hat{u}_{TE_{PEC}}\right]\exp(-j\underline{k}^i \cdot \underline{r}'_{PEC}) \\ &= \underline{J}_{s_{PEC}}^*\exp(-j\underline{k}^i \cdot \underline{r}'_{PEC}) \end{aligned} \tag{1}$$

where ζ_0 is the free-space impedance, $\hat{t}_{PEC} = \hat{n}_{PEC} \times \hat{u}_{TE_{PEC}}$, and $\underline{r}'_{PEC}$ denotes a point on S_{PEC}. Obviously, the magnetic counterpart gives $\underline{J}_{ms_{PEC}} = 0$.

The equivalent PO surface currents on S_{MC} are evaluated according to [31, 32]:

$$\begin{aligned}\underline{J}_{s_{MC}} &= \hat{n}_{MC} \times (\underline{H}^i + \underline{H}^r)\big|_{S_{MC}} \\ &= \frac{1}{\zeta_0}\left[(1-\Gamma_{TE})\,E_{TE_{MC}}^i\sin\beta'\sin\phi'\hat{u}_{TE_{MC}} + (1+\Gamma_{TM})\,E_{TM_{MC}}^i\hat{t}_{MC}\right]\exp(-j\underline{k}^i \cdot \underline{r}'_{MC}) \\ &= \underline{J}_{s_{MC}}^*\exp(-j\underline{k}^i \cdot \underline{r}'_{MC}) \end{aligned} \tag{2}$$

$$\begin{aligned}\underline{J}_{ms_{MC}} &= (\underline{E}^i + \underline{E}^r)\big|_{S_{MC}} \times \hat{n}_{MC} \\ &= \left[(1-\Gamma_{TM})\,E_{TM_{MC}}^i\sin\beta'\sin\phi'\hat{u}_{TE_{MC}} - (1+\Gamma_{TE})\,E_{TE_{MC}}^i\hat{t}_{MC}\right]\exp(-j\underline{k}^i \cdot \underline{r}'_{MC}) \\ &= \underline{J}_{ms_{MC}}^*\exp(-j\underline{k}^i \cdot \underline{r}'_{MC}) \end{aligned} \tag{3}$$

Above expressions contain the electric field components parallel (TM) and perpendicular (TE) to the ordinary plane of incidence defined by the propagation vector of the incident plane wave and the unit vector normal to the lit surface. Such formulations are useful for the evaluation of the considered PO surface currents since they adopt the standard ray-fixed reference frames for the plane wave reflection. Obviously, in order to obtain the UAPO diffracted field in the UTD context, proper transformation matrices must be used in the next section.

The reflection coefficients Γ_{TE} and Γ_{TM} have to be determined for completing the evaluation of $\underline{J}_{s_{MC}}$ and $\underline{J}_{ms_{MC}}$. The ETL circuit is used for this goal in accordance with [18], i.e.,

$$\Gamma_{TM,TE} = \frac{Z_{TM,TE}^{in} - Z_{TM,TE}^0}{Z_{TM,TE}^{in} + Z_{TM,TE}^0} \tag{4}$$

where $Z_{TM}^0 = \zeta_0\cos\theta^i$ and $Z_{TE}^0 = \zeta_0/\cos\theta^i$ are the free-space ETL characteristic impedances with $\cos\theta^i = \sin\beta'\sin\phi'$. The ETL input impedances $Z_{TM,TE}^{in}$ for the DNG MTM layer are given by:

$$Z_{TM,TE}^{in} = jZ_{TM,TE}\tan(k_n d) \tag{5}$$

with $Z_{TM} = k_n/\omega\varepsilon$, $\quad Z_{TE} = \omega\mu/k_n$, and $k_n = -\beta_n - j\alpha_n$ is the propagation factor relevant to the normal to S_{MC}. The interested reader can utilize Eqs. (6)–(9) in [18] to compute β_n and α_n.

3. THE UAPO SOLUTION FOR THE DIFFRACTION CONTRIBUTION

The PO surface currents in Eqs. (1)–(3) are now used as radiating sources on the external faces of the partially coated PEC wedge for evaluating the scattered electric field $\underline{E}^s$ by means of the radiation integral:

$$\begin{aligned}\underline{E}^s \;=\; & -jk_0U_{MC}\iint\limits_{S_{MC}}\left[\left(\underline{\underline{I}}-\hat{R}_{MC}\hat{R}_{MC}\right)\zeta_0\underline{J}_{s_{MC}}+\underline{J}_{ms_{MC}}\times\hat{R}_{MC}\right]G\left(\underline{r},\underline{r}'_{MC}\right)\mathrm{d}S\\ & -jk_0U_{PEC}\iint\limits_{S_{PEC}}\left[\left(\underline{\underline{I}}-\hat{R}_{PEC}\hat{R}_{PEC}\right)\zeta_0\underline{J}_{s_{PEC}}\right]G\left(\underline{r},\underline{r}'_{PEC}\right)\mathrm{d}S\end{aligned}\tag{6}$$

wherein $U_{MC,PEC}$ is equal to 1 or 0 accounting for the illumination of the related surface by the incident plane wave. The Green function $G\left(\underline{r},\underline{r}'\right)=\exp\left(-jk_0|\underline{r}-\underline{r}'|\right)/(4\pi|\underline{r}-\underline{r}'|)$ and $\hat{R}=(\underline{r}-\underline{r}')/|\underline{r}-\underline{r}'|$ depend on the observation point P at $\underline{r}=x\hat{x}+y\hat{y}+z\hat{z}=\underline{\rho}+z\hat{z}$ and the source points at $\underline{r}'_{MC}=x'\hat{x}+z'\hat{z}=\rho'\hat{x}+z'\hat{z}=\underline{\rho}'_{MC}+z'\hat{z}$ and $\underline{r}'_{PEC}=y'\hat{y}+z'\hat{z}=-\rho'\hat{y}+z'\hat{z}=\underline{\rho}'_{PEC}+z'\hat{z}$ $(\rho'>0)$. The symbol $\underline{\underline{I}}$ identifies the 3×3 identity matrix.

According to [18–30], the UAPO approach allows one to isolate the high-frequency diffraction contribution that is enclosed in (6). This is possible by performing useful analytic approximations and integral evaluations.

The next step of the UAPO approach accounts for P lying on the Keller's cone. This permits to use the approximation $\hat{R}_{MC,PEC}\cong\hat{s}=\sin\beta'\cos\phi\,\hat{x}+\sin\beta'\sin\phi\,\hat{y}+\cos\beta'\hat{z}$ ($\hat{s}$ is the unit vector of the diffraction direction on the Keller's cone), thus consenting the following formulation:

$$\underline{E}^s\cong U_{MC}\left[\left(\underline{\underline{I}}-\hat{s}\hat{s}\right)\zeta_0\underline{J}^*_{s_{MC}}+\underline{J}^*_{ms_{MC}}\times\hat{s}\right]I^s_{MC}+U_{PEC}\left[\left(\underline{\underline{I}}-\hat{s}\hat{s}\right)\zeta_0\underline{J}^*_{s_{PEC}}\right]I^s_{PEC}\tag{7}$$

where

$$\begin{aligned}I^s_{MC,PEC} \;=\; & \frac{-jk_0}{4\pi}\iint\limits_{S_{MC,PEC}}\frac{\exp\left(-jk_0\left(\hat{k}^i\cdot\underline{r}'_{MC,PEC}+\left|\underline{r}-\underline{r}'_{MC,PEC}\right|\right)\right)}{\left|\underline{r}-\underline{r}'_{MC,PEC}\right|}\mathrm{d}S\\ =\; & \frac{-jk_0}{4\pi}\int\limits_0^{+\infty}\exp\left(jk_0\rho'\sin\beta'\cos\Phi'_{MC,PEC}\right)I_{z'_{MC,PEC}}\mathrm{d}\rho'\end{aligned}\tag{8}$$

with $\Phi'_{MC}=\phi'$ and $\Phi'_{PEC}=3\pi/2-\phi'$. A proper change of the integration parameter z' gives [11]:

$$I_{z'_{MC,PEC}}=-j\pi\exp\left(-jk_0z\cos\beta'\right)H_0^{(2)}\left(k_0\left|\underline{\rho}-\underline{\rho}'_{MC,PEC}\right|\sin\beta'\right)\tag{9}$$

where $H_0^{(2)}(\cdot)$ is the zeroth order Hankel function of second kind. A useful integral representation of the involved Hankel function is now applied [33]:

$$\begin{aligned}& H_0^{(2)}\left(k_0\left|\underline{\rho}-\underline{\rho}'_{MC,PEC}\right|\sin\beta'\right)\\ =\; & \frac{1}{\pi}\int\limits_C\exp\left(-jk_0\rho\sin\beta'\cos\left(\alpha\mp\Phi_{MC,PEC}\right)\right)\exp\left(jk_0\rho'\sin\beta'\cos\alpha\right)\mathrm{d}\alpha\end{aligned}\tag{10}$$

with $\rho=|\underline{\rho}|$, $\Phi_{MC}=\phi$ and $\Phi_{PEC}=3\pi/2-\phi$. The sign $-$ $(+)$ must be used if $0<\Phi_{MC,PEC}<\pi$ $(\pi<\Phi_{MC,PEC}<2\pi)$. Accordingly, Eq. (8) becomes:

$$\begin{aligned}I^s_{MC,PEC} = & \frac{-k_0}{4\pi}\exp\left(-jk_0z\cos\beta'\right)\\ & \cdot\int\limits_0^{+\infty}\exp\left(jk_0\rho'\sin\beta'\left(\cos\alpha+\cos\Phi'_{MC,PEC}\right)\right)\int\limits_C\exp\left(-jk_0\rho\sin\beta'\cos\left(\alpha\mp\Phi_{MC,PEC}\right)\right)\mathrm{d}\alpha\mathrm{d}\rho'\\ = & \frac{\exp\left(-jk_0z\cos\beta'\right)}{2\sin\beta'}\frac{1}{2\pi j}\int\limits_C\frac{\exp\left(-jk_0\rho\sin\beta'\cos\left(\alpha\mp\Phi_{MC,PEC}\right)\right)}{\cos\alpha+\cos\Phi'_{MC,PEC}}\mathrm{d}\alpha\end{aligned}\tag{11}$$

The last step results from the Sommerfeld-Maliuzhinets' inversion formula [34] and permits to express the above integration in the following form:

$$I^s_{MC,PEC} = \frac{1}{2\pi j}\int_C g(\alpha)\exp\left(\Omega f(\alpha)\right)\mathrm{d}\alpha \quad \Omega = k_0\rho \tag{12}$$

The UAPO approach allows one to extract the diffraction contribution from Eq. (12) by means of the Steepest Descent Method [11]. The application of the Multiplicative Method to the integration along the Steepest Descent Path and the successive asymptotic evaluation of the resulting integral permit to determine the following diffraction term to be used:

$$I^d_{MC,PEC} = \frac{\exp(-j\pi/4)}{2\sqrt{2\pi k_0}} \frac{F_t\left(2k_0 s\sin^2\beta'\cos^2\left(\dfrac{\Phi_{MC,PEC}\pm\Phi'_{MC,PEC}}{2}\right)\right)}{\sin^2\beta'\left[\cos\Phi_{MC,PEC}+\cos\Phi'_{MC,PEC}\right]}\frac{\exp(-jk_0 s)}{\sqrt{s}} \tag{13}$$

where s is the distance from the diffraction point to P (see Fig. 1); $F_t(\cdot)$ is the UTD transition function [5]; and the sign + (−) must be used if $0 < \Phi_{MC,PEC} < \pi$ ($\pi < \Phi_{MC,PEC} < 2\pi$). Accordingly, the UAPO diffraction contribution included in Eq. (7) is given as follows:

$$\underline{E}^d = U_{MC}\left[\left(\underline{\underline{I}}-\hat{s}\hat{s}\right)\zeta_0\underline{J}^*_{s_{MC}} + \underline{J}^*_{ms_{MC}}\times\hat{s}\right]I^d_{MC} + U_{PEC}\left[\left(\underline{\underline{I}}-\hat{s}\hat{s}\right)\zeta_0\underline{J}^*_{s_{PEC}}\right]I^d_{PEC} \tag{14}$$

The above expression can be rewritten in useful local co-ordinate systems as in [5] by adopting a matrix notation, i.e.,

$$\begin{pmatrix} E^d_\beta \\ E^d_\phi \end{pmatrix} = \left[U_{MC}I^d_{MC}\underline{\underline{M}}_{MC} + U_{PEC}I^d_{PEC}\underline{\underline{M}}_{PEC}\right]\begin{pmatrix} E^i_{\beta'} \\ E^i_{\phi'} \end{pmatrix} = \underline{\underline{D}}\begin{pmatrix} E^i_{\beta'} \\ E^i_{\phi'} \end{pmatrix}\frac{\exp(-jk_0 s)}{\sqrt{s}} \tag{15}$$

Appendix contains the expressions of $\underline{\underline{M}}_{MC}$ and $\underline{\underline{M}}_{PEC}$ accounting for the transformation matrices between the involved local co-ordinate systems.

4. VALIDATION OF THE UAPO SOLUTION

Numerical tests are shown in this Section to validate the proposed UAPO solution for the diffracted field. Two sets of figures concerning DNG MTM coatings are reported in the following to prove its ability to counterbalance the GO field discontinuities (Figs. 2 and 3) and to deliver reliable results by using comparisons with Comsol Multiphysics® data (from Fig. 4 to Fig. 9). A circular path is considered as observation domain with $\rho = 5\lambda_0$ (λ_0 is the free-space wavelength) and $0 < \phi < 270°$.

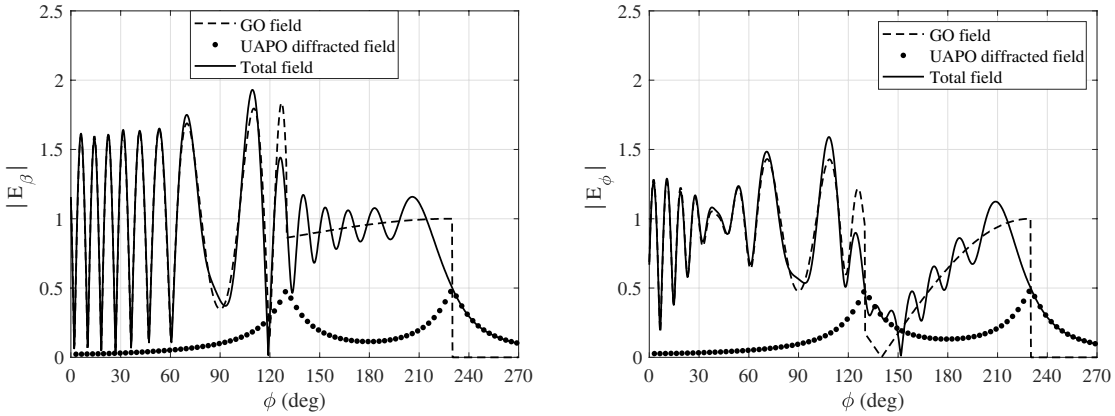

(a) Magnitudes of the β-components (b) Magnitudes of the ϕ-components

Figure 2. Magnitudes of the field components when $\beta' = 70°$, $\phi' = 50°$ and (a) $E^i_{\beta'} = 1$, $E^i_{\phi'} = 0$; (b) $E^i_{\beta'} = 0$, $E^i_{\phi'} = 1$. DNG MTM coating with $d = 0.1\lambda_0$, $\mu_r = -1$, $\varepsilon_r = -(4 + j0.01)$.

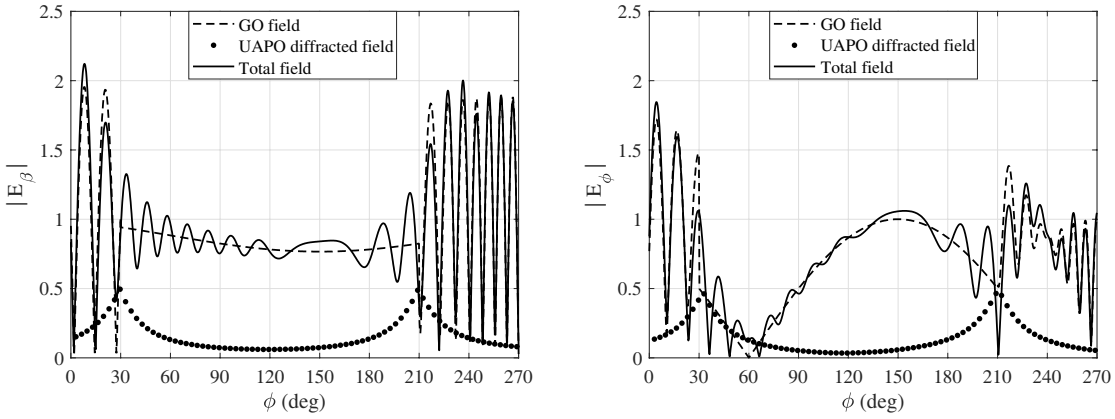

(a) Magnitudes of the β-components (b) Magnitudes of the ϕ-components

Figure 3. Magnitudes of the field components when $\beta' = 70°$, $\phi' = 150°$ and (a) $E^i_{\beta'} = 1$, $E^i_{\phi'} = 0$; (b) $E^i_{\beta'} = 0$, $E^i_{\phi'} = 1$. DNG MTM coating with $d = 0.1\lambda_0$, $\mu_r = -1$, $\varepsilon_r = -(4 + j0.01)$.

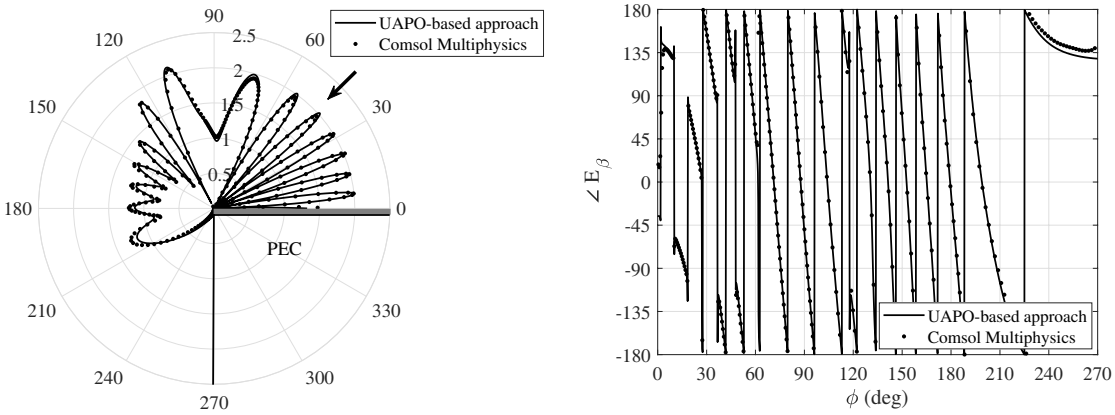

(a) Magnitude of the β-component (b) Phase of the β-component

Figure 4. Magnitude and phase of the field β-component when $\beta' = 90°$, $\phi' = 45°$ and $E^i_{\beta'} = 1$, $E^i_{\phi'} = 0$. DNG MTM coating with $d = 0.1\lambda_0$, $\mu_r = -1$, $\varepsilon_r = -(4 + j0.01)$.

Figures 2 and 3 refer to a DNG MTM coating characterized by $d = 0.1\lambda_0$, $\mu_r = -1$, $\varepsilon_r = -(4+j0.01)$ and consist of two plots: a) β-components of the GO, UAPO and total fields when $E^i_{\beta'} = 1$, $E^i_{\phi'} = 0$; b) ϕ-components of the GO, UAPO and total fields when $E^i_{\beta'} = 0$, $E^i_{\phi'} = 1$. Since Fig. 2 is relevant to $\beta' = 70°$ and $\phi' = 50°$, $U_{MC} = 1$ and $U_{PEC} = 0$ are valid, and the PEC surface does not contribute to the UAPO diffracted field only exhibiting significant peaks at the shadow boundaries of the incident field ($\phi = 230°$) and the reflected field from S_{MC} ($\phi = 130°$). The continuity of the total field in correspondence to such directions reveals that the jumps of the GO field are compensated by the UAPO contribution as expected. Fig. 3 also confirms such a result in the case of shadow boundaries due to the reflections from S_{MC} and S_{PEC} at $\phi = 30°$ and $\phi = 210°$, respectively, since $\beta' = 70°$, $\phi' = 150°$ and $U_{MC} = 1$, $U_{PEC} = 1$.

The second set of figures contains comparisons with Comsol Multiphysics® data when the same DNG MTM coating used in Figs. 2 and 3 is considered in the case of normal incidence ($\beta' = 90°$). Each reported case is organized as follows: a) the magnitude of the UAPO-based total field is compared with the Comsol Multiphysics® counterpart; b) the comparison is made by considering the phase data. The first case refers to $\phi' = 45°$ (only S_{MC} interacts with the incident plane wave), and the comparisons

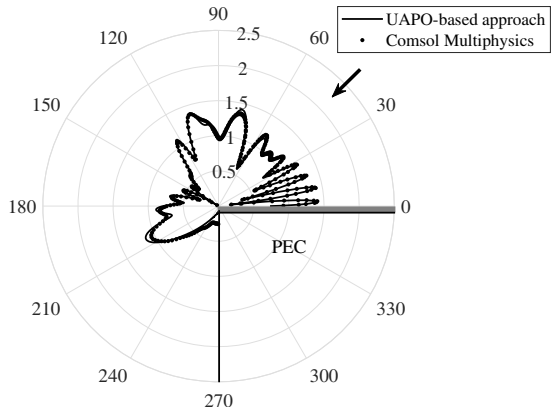

(a) Magnitude of the ϕ-component

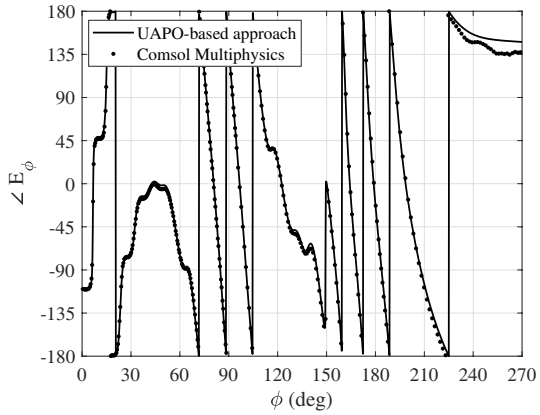

(b) Phase of the ϕ-component

Figure 5. Magnitude and phase of the field ϕ-component when $\beta' = 90°$, $\phi' = 45°$ and $E^i_{\beta'} = 0$, $E^i_{\phi'} = 1$. DNG MTM coating with $d = 0.1\lambda_0$, $\mu_r = -1$, $\varepsilon_r = -(4 + j0.01)$.

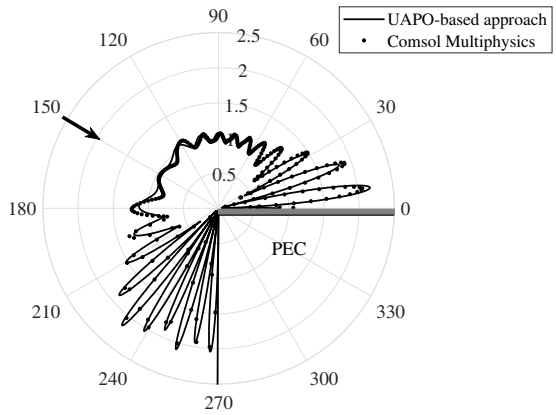

(a) Magnitude of the β-component

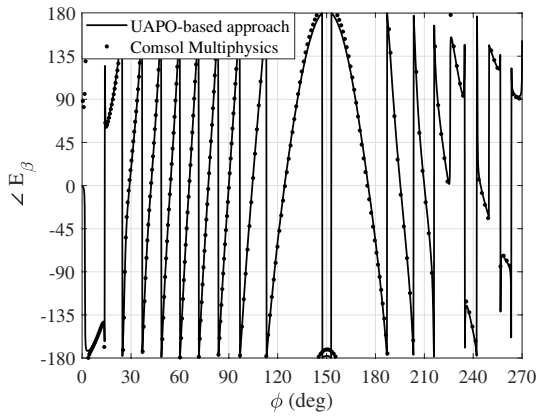

(b) Phase of the β-component

Figure 6. Magnitude and phase of the field β-component when $\beta' = 90°$, $\phi' = 150°$ and $E^i_{\beta'} = 1$, $E^i_{\phi'} = 0$. DNG MTM coating with $d = 0.1\lambda_0$, $\mu_r = -1$, $\varepsilon_r = -(4 + j0.01)$.

are shown in Figs. 4 and 5 with reference to the β- and ϕ-components, respectively. The results show very good agreements. Only the phase values produce evident differences in the angular range from the incident shadow boundary and S_{PEC} since the last is not considered in the UAPO approach. As a matter of fact, if both wedge surfaces are illuminated by the incident plane wave as in the second case ($\phi' = 150°$), the data agree very well on the whole observation path as can be seen in Figs. 6 and 7.

Figures 8 and 9 close the comparisons with Comsol Multiphysics® data. They are relevant to complex values of ε_r and μ_r, i.e., $\varepsilon_r = -(2 + j0.02)$ and $\mu_r = -(7 + j0.05)$, and contain the field β-components when $E^i_{\beta'} = 1$, $E^i_{\phi'} = 0$, and the incidence direction is into the first (see Fig. 8) or second (see Fig. 9) quadrant. It seems that the UAPO approach works very well again, thus assuring reliable results also in such cases.

According to all performed numerical tests, the effectiveness of the UAPO approach is well proved for the considered diffraction problem. It is important to make evident that the performance of the proposed methodology deteriorates when considering the coating thickness greater than a few tenths of the wavelength as pointed out in previous studies. Moreover, the reader must always remember that the UAPO solution for a diffraction problem is an approximate solution, which is based on the PO approximation of equivalent sources.

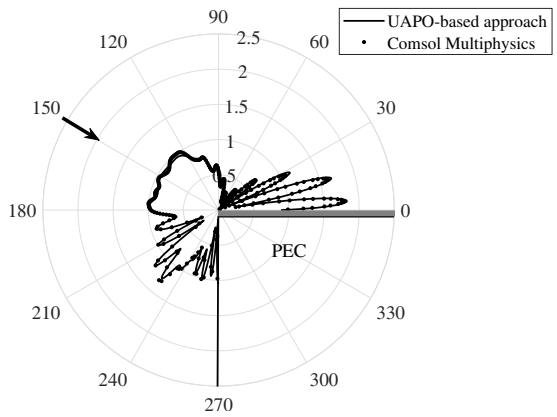

(a) Magnitude of the ϕ-component

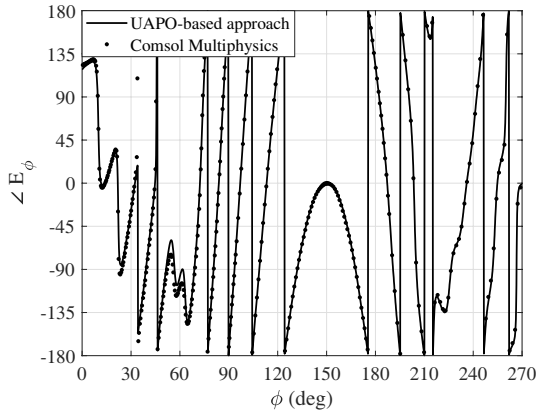

(b) Phase of the ϕ-component

Figure 7. Magnitude and phase of the field ϕ-component when $\beta' = 90°$, $\phi' = 150°$ and $E^i_{\beta'} = 0$, $E^i_{\phi'} = 1$. DNG MTM coating with $d = 0.1\lambda_0$, $\mu_r = -1$, $\varepsilon_r = -(4 + j0.01)$.

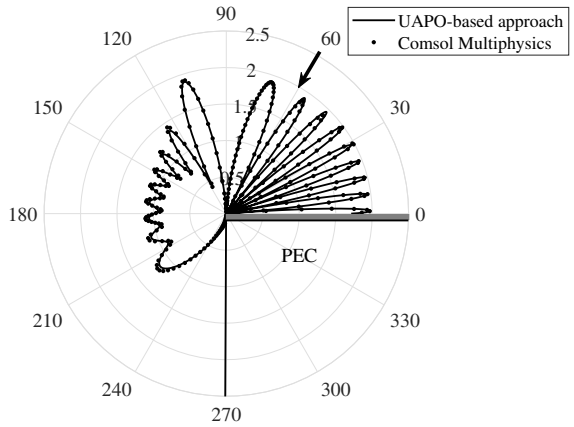

(a) Magnitude of the β-component

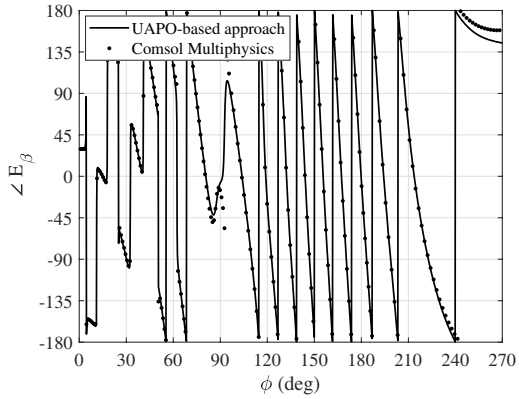

(b) Phase of the β-component

Figure 8. Magnitude and phase of the field β-component when $\beta' = 90°$, $\phi' = 60°$ and $E^i_{\beta'} = 1$, $E^i_{\phi'} = 0$. DNG MTM coating with $d = 0.1\lambda_0$, $\mu_r = -(7 + j0.05)$, $\varepsilon_r = -(2 + j0.02)$.

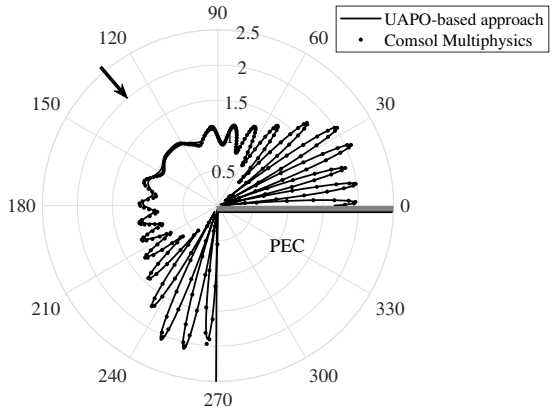

(a) Magnitude of the β-component

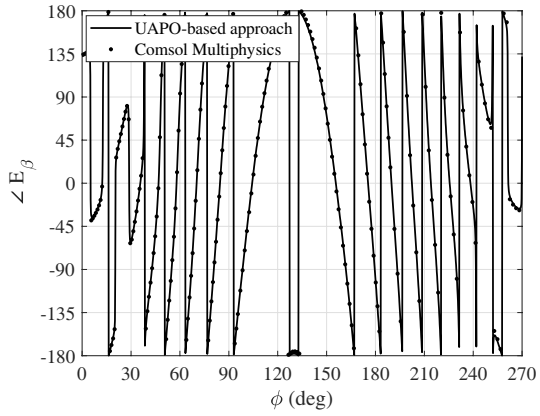

(b) Phase of the β-component

Figure 9. Magnitude and phase of the field β-component when $\beta' = 90°$, $\phi' = 130°$ and $E^i_{\beta'} = 1$, $E^i_{\phi'} = 0$. DNG MTM coating with $d = 0.1\lambda_0$, $\mu_r = -(7 + j0.05)$, $\varepsilon_r = -(2 + j0.02)$.

5. CONCLUSIONS

The UAPO solution for evaluating the diffracted field by a partially coated PEC wedge with apex angle equal to 90° has been proposed. Its formulation of the diffraction matrix in the UTD framework is simple to use and does not require computing differential/integral equations or special functions. Moreover, reliable results can be obtained as well assessed by comparisons with Comsol Multiphysics® data. On the other hand, a prudent user must always keep in mind that the UAPO solution to a diffraction problem is an approximate solution, which is based on the PO approximation of equivalent surface currents.

APPENDIX A.

The matrix $\underline{\underline{M}}_{MC}$ can be so formulated:

$$\underline{\underline{M}}_{MC} = \underline{\underline{M}}_1 \left[\underline{\underline{M}}_2\underline{\underline{M}}_4\underline{\underline{M}}_5 + \underline{\underline{M}}_3\underline{\underline{M}}_4\underline{\underline{M}}_6\right] \underline{\underline{M}}_7 \tag{A1}$$

wherein

$$\underline{\underline{M}}_1 = \begin{pmatrix} \cos\beta'\cos\phi & \cos\beta'\sin\phi & -\sin\beta' \\ -\sin\phi & \cos\phi & 0 \end{pmatrix} \tag{A2}$$

$$\underline{\underline{M}}_2 = \begin{pmatrix} 1-\sin^2\beta'\cos^2\phi & -\sin\beta'\cos\beta'\cos\phi \\ -\sin^2\beta'\sin\phi\cos\phi & -\sin\beta'\cos\beta'\sin\phi \\ -\sin\beta'\cos\beta'\cos\phi & \sin^2\beta' \end{pmatrix} \tag{A3}$$

$$\underline{\underline{M}}_3 = \begin{pmatrix} 0 & -\sin\beta'\sin\phi \\ -\cos\beta' & \sin\beta'\cos\phi \\ \sin\beta'\sin\phi & 0 \end{pmatrix} \tag{A4}$$

$$\underline{\underline{M}}_4 = \frac{1}{\sqrt{1-\sin^2\beta'\sin^2\phi'}} \begin{pmatrix} -\cos\beta' & -\sin\beta'\cos\phi' \\ -\sin\beta'\cos\phi' & \cos\beta' \end{pmatrix} \tag{A5}$$

$$\underline{\underline{M}}_5 = \begin{pmatrix} 0 & (1-\Gamma_{TE})\sin\beta'\sin\phi' \\ 1+\Gamma_{TM} & 0 \end{pmatrix} \tag{A6}$$

$$\underline{\underline{M}}_6 = \begin{pmatrix} (1-\Gamma_{TM})\sin\beta'\sin\phi' & 0 \\ 0 & -1-\Gamma_{TE} \end{pmatrix} \tag{A7}$$

$$\underline{\underline{M}}_7 = \frac{1}{\sqrt{1-\sin^2\beta'\sin^2\phi'}} \begin{pmatrix} \cos\beta'\sin\phi' & \cos\phi' \\ -\cos\phi' & \cos\beta'\sin\phi' \end{pmatrix} \tag{A8}$$

Note that $\underline{\underline{M}}_5$ and $\underline{\underline{M}}_6$ account for the expressions of $\underline{J}^*_{s_{MC}}$ and $\underline{J}^*_{ms_{MC}}$, respectively.

The matrix $\underline{\underline{M}}_{PEC}$ can be expressed by following the same practice, i.e.,

$$\underline{\underline{M}}_{PEC} = \underline{\underline{M}}_1\underline{\underline{N}}_2\underline{\underline{N}}_3\underline{\underline{N}}_4\underline{\underline{N}}_5 \tag{A9}$$

with

$$\underline{\underline{N}}_2 = \begin{pmatrix} 1-\sin^2\beta'\cos^2\phi & -\sin^2\beta'\sin\phi\cos\phi & -\sin\beta'\cos\beta'\cos\phi \\ -\sin^2\beta'\sin\phi\cos\phi & 1-\sin^2\beta'\sin^2\phi & -\sin\beta'\cos\beta'\sin\phi \\ -\sin\beta'\cos\beta'\cos\phi & -\sin\beta'\cos\beta'\sin\phi & \sin^2\beta' \end{pmatrix} \tag{A10}$$

$$\underline{\underline{N}}_3 = \frac{1}{\sqrt{1-\sin^2\beta'\sin^2\phi'}} \begin{pmatrix} 0 & 0 \\ -\cos\beta' & -\sin\beta'\sin\phi' \\ -\sin\beta'\sin\phi' & \cos\beta' \end{pmatrix} \tag{A11}$$

$$\underline{\underline{N}}_4 = \begin{pmatrix} 0 & -2\sin\beta'\cos\phi' \\ 2 & 0 \end{pmatrix} \tag{A12}$$

$$\underline{\underline{N}}_5 = \frac{1}{\sqrt{1-\sin^2\beta'\sin^2\phi'}} \begin{pmatrix} -\cos\beta'\sin\phi' & \sin\phi' \\ -\sin\phi' & -\cos\beta'\sin\phi' \end{pmatrix} \tag{A13}$$

REFERENCES

1. Engheta, N. and R. W. Ziolkowski, Ed., *Metamaterials: Physics and Engineering Explorations*, Wiley & Sons, USA, 2006.
2. Sakoda, K. (ed.), *Electromagnetic Metamaterials: Modern Insights into Macroscopic Electromagnetic Fields*, Springer, Singapore, 2019.
3. Marquéz, R., F. Martin, and M. Sorolla, *Metamaterials with Negative Parameters: Theory, Design and Microwave Applications*, Wiley & Sons, USA, 2008.
4. Basdemir, H. D., "Scattering of plane waves by a rational half-plane between DNG media," *Optik*, Vol. 179, 47–53, 2019.
5. Kouyoumjian, R. G. and P. H. Pathak, "A uniform geometrical theory of diffraction for an edge in a perfectly conducting surface," *Proc. IEEE*, Vol. 62, 1448–1461, 1974.
6. Tiberio, R., G. Pelosi, and G. Manara, "A uniform GTD formulation for the diffraction by a wedge with impedance faces," *IEEE Trans. Antennas Propag.*, Vol. 33, 867–873, 1985.
7. Senior, T. B. A. and J. L. Volakis, "Scattering by an imperfect right-angled wedge," *IEEE Trans. Antennas Propag.*, Vol. 34, 681–689, 1986.
8. Rojas, R. G., "Electromagnetic diffraction of an obliquely incident plane wave field by a wedge with impedance faces," *IEEE Trans. Antennas Propag.*, Vol. 36, 956–970, 1988.
9. Syed, H. H. and J. L. Volakis, "An approximate solution for scattering by an impedance wedge at skew incidence," *Radio Sci.*, Vol. 3, 505–524, 1995.
10. Osipov, A. V. and T. B. A. Senior, "Diffraction by a right-angled impedance wedge," *Radio Sci.*, Vol. 43, RS4S02, 2008.
11. Senior, T. B. A. and J. L. Volakis, *Approximate Boundary Conditions in Electromagnetics*, IEE, Stevenage, 1995.
12. Daniele, V. G. and G. Lombardi, "Wiener-Hopf solution for impenetrable wedges at skew incidence," *IEEE Trans. Antennas Propag.*, Vol. 54, 2472–2485, 2006.
13. Lyalinov, M. A. and N. Y. Zhu, "Diffraction of a skew incident plane electromagnetic wave by an impedance wedge," *Wave Motion*, Vol. 44, 21–43, 2006.
14. Holm, P. D., "A new heuristic UTD diffraction coefficient for nonperfectly conducting wedge," *IEEE Trans. Antennas Propag.*, Vol. 48, 1211–1219, 2000.
15. El-Sallabi, H. M. and P. Vainikainen, "Improvements to diffraction coefficient for non-perfectly conducting wedges," *IEEE Trans. Antennas Propag.*, Vol. 53, 3105–3109, 2005.
16. Nechayev, Y. I. and C. C. Constantinou, "Improved heuristic diffraction coefficients for an impedance wedge at normal incidence," *IEE Proc. — Microw. Antennas Propag.*, Vol. 153, 125–132, 2006.
17. Basdemir, H. D., "Diffraction by a right angle impedance wedge between left- and right-handed media," *Journal of Electromagnetic Waves and Applications*, Vol. 34, No. 7, 869–880, 2020.
18. Gennarelli, G. and G. Riccio, "Diffraction by a planar metamaterial junction with PEC backing," *IEEE Trans. Antennas Propag.*, Vol. 58, 2903–2908, 2010.
19. Ferrara, F., C. Gennarelli, R. Guerriero, G. Riccio, and C. Savarese, "A UAPO diffraction contribution to take into account the edge effects in microstrip reflectarrays," *Electromagn.*, Vol. 26, 461–471, 2006.
20. Gennarelli, G. and G. Riccio, "A uniform asymptotic solution for diffraction by a right-angled dielectric wedge," *IEEE Trans. Antennas Propag.*, Vol. 59, 898–903, 2011.
21. Gennarelli, G. and G. Riccio, "Plane-wave diffraction by an obtuse-angled dielectric wedge," *J. Opt. Soc. Am. A*, Vol. 28, 627–632, 2011.
22. Gennarelli, G. and G. Riccio, "Useful solutions for plane wave diffraction by dielectric slabs and wedges," *Int. J. Antennas Propag.*, 1–7, 2012.
23. Gennarelli, G. and G. Riccio, "Diffraction by 90° penetrable wedges with finite conductivity," *J. Opt. Soc. Am. A*, Vol. 31, 21–25, 2014.

24. Gennarelli, G., M. Frongillo, and G. Riccio, "High-frequency evaluation of the field inside and outside an acute-angled dielectric wedge," *IEEE Trans. Antennas Propag.*, Vol. 63, 374–378, 2015.
25. Frongillo, M., G. Gennarelli, and G. Riccio, "Diffraction by a structure composed of metallic and dielectric 90° blocks," *IEEE Antennas Wireless Propag. Lett.*, Vol. 17, 881–885, 2018.
26. Frongillo, M., G. Gennarelli, and G. Riccio, "Plane wave diffraction by arbitrary-angled lossless wedges: High-frequency and time-domain solutions," *IEEE Trans. Antennas Propag.*, Vol. 66, 6646–6653, 2018.
27. Frongillo, M., G. Gennarelli, and G. Riccio, "Diffraction by a dielectric wedge on a ground plane," *Progress In Electromagnetics Research M*, Vol. 82, 9–18, 2019.
28. Gennarelli, G. and G. Riccio, "On the accuracy of the UAPO solution for the diffraction by a PEC — DNG metamaterial junction," *IEEE Antennas Wireless Propag. Lett.*, Vol. 19, 581–585, 2020.
29. Gennarelli, G. and G. Riccio, "High-frequency diffraction contribution by planar metallic — DNG metamaterial junctions," *Int. J. Microw. Wireless Tech.*, 1–6, 2020.
30. Frongillo, M., G. Gennarelli, and G. Riccio, "Useful solutions for the plane wave diffraction by a configuration of dielectric and metallic acute-angled wedges," *Int. J. Comm. Antenna Propag.*, Vol. 10, 68–75, 2020.
31. Meana, J. G., J. A. Martinez-Lorenzo, F. Las-Heras, and C. Rappaport, "Wave scattering by dielectric and lossy materials using the modified equivalent current approximation (MECA)," *IEEE Trans. Antennas Propag.*, Vol. 58, 3757–3760, 2010.
32. Meana, J. G., J. A. Martinez-Lorenzo, and F. Las-Heras, "High frequency techniques: The physical optics approximation and the modified equivalent current approximation (MECA)," *Electromagnetic Waves Propagation in Complex Matter*, A. Kishk (ed.), 207–230, Intech, Croatia, 2011.
33. Clemmow, P. C., *The Plane Wave Spectrum Representation of Electromagnetic Fields*, Oxford University Press, UK, 1996.
34. Maliuzhinets, G. D., "Inversion formula for the Sommerfeld integral," *Soviet Physics Doklady*, Vol. 3, 52–56, 1958.